Biophysical Journal
Article

Biophysical Society

PSI-SMALP, a Detergent-free Cyanobacterial Photosystem I, Reveals Faster Femtosecond Photochemistry

Dmitry A. Cherepanov,[1] Nathan G. Brady,[2] Ivan V. Shelaev,[1] Jon Nguyen,[2] Fedor E. Gostev,[1] Mahir D. Mamedov,[3] Victor A. Nadtochenko,[1,*] and Barry D. Bruce[2,4,*]

[1]N. N. Semenov Federal Research Center for Chemical Physics, Russian Academy of Sciences, Moscow, Russia; [2]Biochemistry and Cellular and Molecular Biology Department, University of Tennessee, Knoxville, Tennessee; [3]A. N. Belozersky Institute of Physical-Chemical Biology, Moscow State University, Moscow, Russia; and [4]Energy Science & Engineering Program, The Bredesen Center, University of Tennessee, Knoxville, Tennessee

ABSTRACT Cyanobacterial photosystem I (PSI) functions as a light-driven cyt c_6-ferredoxin/oxidoreductase located in the thylakoid membrane. In this work, the energy and charge transfer processes in PSI complexes isolated from *Thermosynechococcus elongatus* via conventional n-dodecyl-β-D-maltoside solubilization (DM-PSI) and a, to our knowledge, new detergent-free method using styrene-maleic acid copolymers (SMA-PSI) have been investigated by pump-to-probe femtosecond laser spectroscopy. In DM-PSI preparations excited at 740 nm, the excitation remained localized on the long-wavelength chlorophyll forms within 0.1–20 ps and revealed little or no charge separation and oxidation of the special pair, P700. The formation of ion-radical pair $P700^{+}A1^{-}$ occurred with a characteristic time of 36 ps, being kinetically controlled by energy transfer from the long-wavelength chlorophyll to P_{700}. Quite surprisingly, the detergent-free SMA-PSI complexes upon excitation by these long-wave pulses undergo an ultrafast ($<$100 fs) charge separation in $\sim$45% of particles. In the remaining complexes ($\sim$55%), the energy transfer to P_{700} occurred at $\sim$36 ps, similar to the DM-PSI. Both isolation methods result in a trimeric form of PSI, yet the SMA-PSI complexes display a heterogenous kinetic behavior. The much faster rate of charge separation suggests the existence of an ultrafast pathway for charge separation in the SMA-PSI that may be disrupted during detergent isolation.

SIGNIFICANCE Photosystem I is a remarkably robust reaction center that is key to solar energy conversion on Earth. Here, utilizing styrene-maleic acid alternating copolymers to form native nanodiscs that retain the thylakoid lipids, we find by pump-to-probe femtosecond spectroscopy an ultrafast charge separation event within the reaction center that is lost during detergent isolation. The ultrafast ($<$100 fs) charge separation was observed in 45% of detergent-free styrene-maleic acid-photosystem I complexes excited by long-wave pulses, whereas in the rest, the energy trapping occurred at 36 ps, as in the preparations obtained with a detergent solubilization. These data suggest that this method preserves a more native-like conformation of the protein complex, therefore offering a more authentic environment for biophysical studies and biohybrid device applications.

INTRODUCTION

Photosystem I (PSI) is a membrane-spanning protein complex that contains 12 individual subunits and $\sim$120 cofactors. PSI is one of the key enzymes of the photosynthetic electron-transfer chain, which catalyzes the light-driven one-electron transfer from peripheral protein donor, plastocyanin, and/or cytochrome c_6 to ferredoxin and/or flavodoxin. The crystallographic structure of *Thermosynechococcus elongatus* PSI complexes with a resolution of 2.5 Å (1) led to an accurate model for the architecture of proteins, cofactors, and pigments in that system. Cyanobacterial PSI assembles into a trimer with a C3 axis of symmetry. Each complex, in turn, is a heterodimer formed by symmetrically and homologously related core subunits, PsaA and B. This geometry leaves both the C3 and C2 symmetry axis perpendicular to the membrane plane, with the C2 axis passing through a special dimer of P_{700} chlorophyll (Chl) on the donor side and through an iron-sulfur cluster F_X on the acceptor side. All redox cofactors except terminal

Submitted June 20, 2019, and accepted for publication November 26, 2019.

*Correspondence: nadtochenko@gmail.com or bbruce@utk.edu

Editor: Elsa Yan.

https://doi.org/10.1016/j.bpj.2019.11.3391

iron-sulfur clusters F_A/F_B are located within PsaA or PsaB core subunits in a pseudosymmetrical manner and form two (A and B) branches for potential electron transfer. The two cofactor branches of the electron-transfer chain merge onto the interpolypeptide iron-sulfur cluster F_X. The two terminal electron acceptors F_A and F_B are [4Fe-4S] clusters located on the stromal surface coordinated via the subunit PsaC. In addition, PSI also coordinates 96 Chl *a* molecules and 22 molecules of β-carotene, which serve as antenna pigments (1). In contrast to the bacterial and photosystem II (PSII) reaction center (RC) complexes, the structure of PSI makes it impossible to biochemically separate the Chl molecules associated with PSI RCs from those Chl molecules functioning as light-harvesting antennae molecules.

Recently, the energy and electron transfer reactions in PSI have been studied using various ultrafast techniques, including pump-probe absorption spectroscopy (2–6). However, to date, the kinetics of the primary charge separation in PSI remain controversial (7–11). Thus, after absorption of light by integral antenna pigments, the excitation energy is efficiently transferred to an RC, where the light-induced charge separation into an ion-radical pair between a special pair of Chl, P_{700}, and the primary electron acceptor A_0 occur. The electron from accessory chlorophyll A_0 is further transferred to the phylloquinone (A_1) and finally to the F_A/F_B via interprotein iron-sulfur cluster F_X. Most of the previous studies put the primary charge separation step from P_{700}* to A_0 in PSI RCs in the 0.8–4 ps time range, and the subsequent electron transfer from primary electron acceptor A_0 to the secondary electron acceptor A_1 was suggested to occur in the 10–50 ps range (2,12–14). However, a number of studies (4,9) have shown that in purified PSI complexes from cyanobacteria *Synechocystis* sp. PCC 6803 after preferential excitation of P_{700} and A_0, formation of primary radical pair $P_{700}{}^{+}A_0{}^{-}$ occurs within 100 fs, and the formation of $P_{700}{}^{+}A_1{}^{-}$ has a characteristic time of ~25 ps.

Energy transfer processes between the light-harvesting antenna chlorophylls and the special pair of chlorophyll P_{700} of the PSI RC have been the subject of many years of research. In the simplest version, the kinetic scheme of the energy transfer processes and the charge separation reactions in RC can be represented by Scheme 1.

The organization of pigments within protein complex provides for an effective energy transfer in the antenna and delivery of the excitation energy to the RC, where the charge separation takes place. The efficiency of energy transfer through the system of exciton-coupled cofactors is controlled by their spatial organization (distances between pigments and angles between the dipole transition vectors), as well as by the excitation energies of the lowest Q_Y electronic transition of chlorophyll (15). The electron donor in PSI is a special pair of Chl molecules, P_{700}, whose Q_Y band has a maximum near 700 nm at the red edge of the

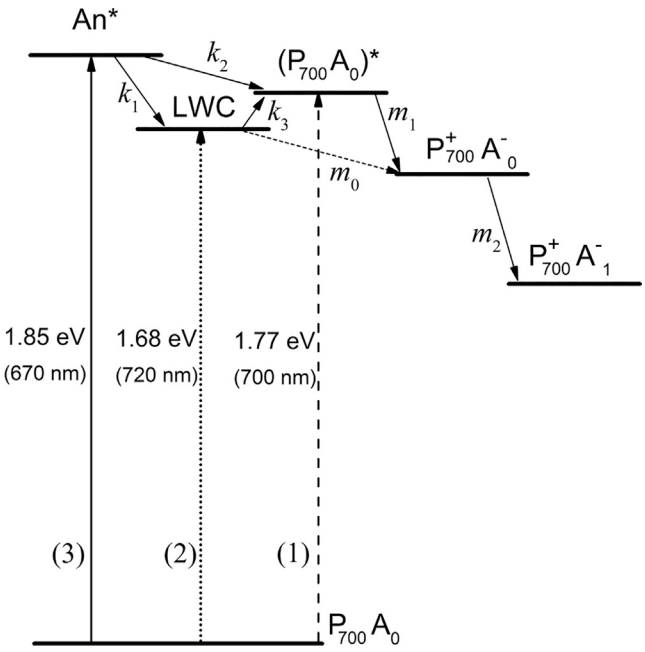

SCHEME 1 The energy diagram and main photoinduced electronic transitions in the PSI from *T. elongatus*. An* represents the majority of the antenna chlorophyll (absorbance ~670 nm), and LWC represents the long-wavelength chlorophyll (absorbance ~720 nm).

PSI absorption spectrum. In the antennae of many cyanobacteria, there are long-wavelength forms of chlorophyll (LWCs), which absorb in the far-red edge of spectrum below the P700 special pair. In PSI from *T. elongatus*, three LWCs—C-708, C-715, and C-719—were detected (16).

Generally, the photochemical production of the oxidized special pair ($P_{700}{}^{+}$) may occur by three alternative pathways. The first path is via the direct excitation of the special pair (*dashed arrow (1)* in Scheme 1). In PSI complexes from *Synechocystis* sp. PCC 6803, which contain a minimal number of LWCs, an ultrafast formation of the ion-radical state $(P_{700}A_0)^* \rightarrow P_{700}{}^{+}A_0{}^{-}$ was revealed upon excitation in the far-red region (4,9), so the assessed lifetime of ~100 fs may be considered as an estimation of the respective rate constant $m_1 = 10^{13}\ s^{-1}$.

The second route to charge separation entails the migration of energy from LWCs to the RC (*dotted arrow (2)* in Scheme 1). When following uphill via the excited state $(P_{700}A_0)^*$, this process requires an activation energy of ~50 meV. In PSI complexes from *Chroococcidiopsis thermalis* PCC 7203, the energy transfer occurred at 97 ps (6), so the assessed rate constant of excitation migration from the LWC to P_{700}, $k_3 = 10^{10}\ s^{-1}$, was slower than the rate of the secondary electron-transfer reaction $m_2 = 4 \times 10^{10}\ s^{-1}$ (2). Further, a slow charge separation was observed at cryogenic temperatures in PSI from *T. elongatus* and *Arthrospira platensis*, indicating the possibility of a direct, activationless transition from the excited LWC to a suggested charge transfer (CT) state via a superexchange

mechanism (the rate constant m_0) (17) similar to the mechanism proposed for purple bacteria (18). Lastly, energy absorbed by the high-energy chlorophyll in antenna (An*) can migrate to the LWC in the time range of few picoseconds (6,19), so the effective rate constant k_1 has magnitude of 3×10^{11} s^{-1}. In addition, a direct pathway of energy transfer from An* to P_{700} (the rate constant k_2) might be considered as a potential alternative.

The LWC molecules operate as energy traps because the ratio of the forward/backward rate constants of energy transfer between chlorophyll molecules 1 and 2 obeys the Boltzmann distribution $k_{12}/k_{21} = \exp(-\Delta E_{12}/k_B T)$, where $\Delta E_{12} = E_2 - E_1$ is the difference between the energies of their excited states. For this reason, the disturbance of the native conformation of PSI during isolation procedure can significantly affect the energy transfer dynamics and charge separation kinetics. In isolated cyanobacterial PSI complexes, detergents can destroy a two-layer structure and form micellar structures around the hydrophobic transmembrane regions of the protein. Although this approach has yielded many results in the detergent-solubilized state, membrane proteins tend to have limited stability and often exhibit much reduced activity when compared with native forms (20). This is the result of the delicate balance that needs to be struck to achieve efficient extraction yield without denaturing the protein.

Recently, the use of detergentless solubilization procedures for membrane proteins has found increasing interest (20–23). The use of SMA copolymers to extract and purify transmembrane proteins while retaining their native bilayer environment overcomes many of the disadvantages associated with conventional detergent-based procedures. This approach has huge potential for the future of membrane protein structural and functional studies. The SMA disk structure is well suited for many biophysical and spectroscopic techniques (24–27), as well as structural studies using electron microscopy (26,28).

In this work, for the first time, to our knowledge, comparative analysis of the fast energy and charge transfer processes of *T. elongatus* PSI complexes prepared using n-dodecyl-β-D-maltoside (DM-PSI) and styrene-maleic acid (SMA-PSI) was carried out. We studied the forward and back energy transfer dynamics between different chlorophyll forms in antenna and the special pair P_{700} in the two PSI preparations and the subsequent charge separation reactions in the RC.

MATERIALS AND METHODS

T. elongatus cells were grown in a 25 L airlift bioreactor (Photon Systems Instruments, Drásov, Czech Republic) in BG-11 media at 45°C. The bioreactor incorporated back panel illumination containing 680 nm red light and full-spectrum white-light light-emitting diodes with a combined irradiance of 50 μmol photons/m^2/s. Cells were pelleted at 12,000 $\times$ *g* and stored in −80°C before lysis.

The PSI isolation methods are described in detail by Brady et al. (29). Briefly, PSI isolation with DM and SMA began with resuspension of the cell pellet in 50 mM MES-NaOH (pH 6.5) with 10 mM $CaCl_2$ and 10 mM $MgCl_2$ (Buffer A) containing 0.5 M sorbitol. Lysis of *T. elongatus* cells was achieved using a French press at 1500 bar. The lysate was then spun down at 12,000 $\times$ *g* to separate unbroken cells. Thylakoid membranes were pelleted at 180,000 $\times$ *g* in a fixed angle rotor for 30 min. Thylakoid membranes for DM solubilization were gently resuspended in Buffer A to a concentration of 1 mg Chl/mL and homogenized using a Kimble Dounce homogenizer (DWK LIFE SCIENCES LLC, Millville, NJ). After each wash, thylakoid membranes were pelleted at 180,000 $\times$ *g*. The final resuspension diluted the thylakoids to 1 mg Chl/mL in Buffer A with 12.5% (w/v) glycerol. Thylakoid membranes for solubilization with SMA followed the same wash protocol, substituting Buffer A for 50 mM Tris-Cl (pH 9.5) (room temperature) with 125 mM KCl (SMA Buffer). Solubilization of washed thylakoids was carried out at 0.6% (w/v) DM, 25°C for 1 h without agitation and 1.7% SMA (SMA 1440 from Cray Valley, Exton, PA), 40°C for 3 h on a rotating table at 300 rpm, respectively. Thylakoid washing and solubilization steps were carried out in relative darkness for both isolation methods. Protein isolates remained in the supernatant after a final centrifugation at 180,000 $\times$ *g* for both DM and SMA solubilizations. The soluble fraction after incubation of *T. elongatus* thylakoid membranes with DDM (n-dodecyl-B-D-maltoside) or SMA was loaded on to a 10–30% sucrose gradient and centrifuged at 150,000 $\times$ *g* for 20 h. Chlorophyll fluorescence was performed at 77 K using a PTI Quantamaster dual-channel fluorometer (HORIBA, Minami-ku, Kyoto, Japan). The samples were excited with 420 nm light. and the emission spectra were scanned from 550 to 800 nm with 0.5 nm steps and a 1 nm slit width. The resulting spectra are the average of four traces. Absorbance spectra were obtained using a Thermo Fisher Scientific Evolution 300 dual-beam ultraviolet (UV)-visible spectrophotometer (Waltham, MA). Isolated PSI complexes were analyzed by blue native polyacrylamide gel electrophoresis (BN-PAGE). 4–16% BN-PAGE precast gels (Invitrogen, Carlsbad, CA) were used, following established protocols (30,31). SDS-PAGE analysis was performed using a 18–24% tris-glycine gradient containing 6 M urea as described by Kubota et al. (32).

The experimental setup was described elsewhere (4). Briefly, time-resolved difference absorption spectra $\Delta A(\lambda, t)$ were measured by a pump-probe method. The excitation pulses were centered at wavelengths of 740 and 670 nm. In the experiments with excitation at 740 nm, the pulses had energy of 100–200 nJ and a duration of 26 fs. In the case of excitation pulses at 670 nm, the pulse spectrum was filtered by the SLM (spatial light modulator) modulator so that spectral components redder than 680 nm were absent. In this case, the excitation pulse duration was 34 fs, and the energy was 40 nJ. The excitation pulses were focused in a 0.5-mm-thick cuvette with thin quartz glasses (150 μm thick) into a spot with a diameter of 180 μm. A pulse of white continuum focused in a spot of 120 μm diameter was used as a probe pulse. Polarizations of the pump and probe pulses were oriented by a magic angle of 54.7°. The pulse repetition rate was 100 Hz. The sample was circulated by a micropump through a cuvette at a rate sufficient to completely replace the exposed volume between the pulses. In this case, the samples were cooled to +6°C. The zero time delay between the pump pulse and corresponding spectral component λ of the probe pulse was corrected by a method described elsewhere (9,33). The difference absorption spectra $\Delta A(\lambda, t) = A(\lambda, t) - A_0(\lambda)$ obtained by the pump-probe femtosecond laser photolysis are the difference of between the spectrum of the PS1 $A(\lambda, t)$ at the time delay t and the absorption spectrum of PSI without excitation $A_0(\lambda)$.

Particular attention was given to the "coherence spike" or "coherent artifact," which is seen at the beginning of the evolution during pump-probe overlap. Coherence spikes arise from a cross-phase modulation of the probe pulse in the presence of strong pump pulse (34), two-photon absorption of pump and probe photons at high light flux density (35), and electronic dephasing due to dynamic Stokes shifts (solvent fluctuations and intramolecular bath modes) (36). The form and magnitude of the artifacts depended nonlinearly on the pump energy and varied at different probe wavelengths, so the instrumental response function could not be modeled

with sufficient accuracy. Fig. S1 shows the transient optical dynamics of DM-PSI at short delays -200 fs $< t_d <$ 500 fs under excitation by low-energy 670 nm and high-energy 740 nm pulses. At low-energy 670 nm excitation, the coherent artifacts disturbed the kinetics at delays $t_d \leq 80$ fs, whereas at high-energy 740 nm excitation, the coherent artifacts were observed at $t_d \leq 120$ fs (Fig. S1). In this work, the data were analyzed for time delays after the "coherence spike."

CONTIN analysis of optical dynamics

The spectral dynamics of PSI was expressed by two-dimensional matrices of the form $\Delta A(\lambda_n, t)$ in the spectral range of 430–720 nm and in the time interval of 0.05–500 ps. At each wavelength λ_n, the spectral dynamics $y_t = \Delta A(\lambda_n, t)$ was discretized at the time arrays $(t_1,\ldots,t_M)$ of the dimension M and analyzed with the CONTIN software (37). CONTIN is a program invented for solution of noisy ill-posed linear operator equations, including Laplace transforms of relaxation dynamics. This means that the inversion of these linear equations results in a large number of possible solutions with arbitrarily large deviations from each other. The method implements the inverse Laplace transform to deconvolute nonmonotonous kinetics (y_t) into a spectrum of exponential components, with the characteristic times τ_k ($k = 1,\ldots,N_\tau$) evenly spaced in the logarithmic timescale. CONTIN employs Tikhonov-Phillips regularization, which minimizes the sum of the squares of the discretized second derivatives of the solution, resulting in a quasicontinuous spectrum with the local smoothness determined by the regularizing parameter α. Namely, for a given relaxation kinetics $Y_\lambda(t)$, CONTIN suggests an array of solutions F_ν ($\nu = 1,\ldots,N$)

$$F_\nu = \sum_k a_{\nu,k} \times e^{-t/\tau_k}, \tag{1}$$

where $a_{\nu,k}$ is the amplitude of exponential component $\exp(-t/\tau_k)$ obtained at the given value α_ν of the regularizing parameter. The residual of solution ν is

$$r_{\nu,t} = y_t - \sum_k a_{\nu,k} \times e^{-\frac{t}{\tau_k}}. \tag{2}$$

In the absence of prior information regarding the shape of kinetic spectrum, CONTIN suggests an "optimal" solution with the most statistically reliable α-value. In particular, an assumption on the non-negative sign of amplitudes $a_{\nu,k}$ can be imposed for some components k. In the common mode of CONTIN implementation, the regularization parameter is chosen independently for transient kinetics $Y_\lambda(t)$ at each wavelength λ on the basis of an F-test. However, this procedure produces spectra that deviate widely from each other for close λ-values. To obtain a quasicontinuous behavior of solution against λ, an additional regularization criterium should be introduced. In the case of this study, an additional criterion was used to select the appropriate α-value, namely, the kinetics at a given wavelength interval $\lambda_n \pm 1$ nm ($n = 1,\ldots,N_\lambda$) should have the minimal dispersion of the spectral profiles. The vector of optimal solutions $[\nu] = (\nu_1,\ldots,\nu_N)$ was found thereby by minimizing the discrepancy function

$$S_{[\nu]} = \sum_i \sigma^2_{\nu_i} + \varepsilon \times \sum_{i,k} \left(a_{\nu_i,k} - \overline{a}_{\nu_i,k}\right)^2. \tag{3}$$

Here, $\sigma^2_{\nu_i} = (M - N_t)^{-1} \sum_t \left| r_{\nu_i,t} \right|^2$ is the mean-square error of CONTIN solution ν_i the for i-th kinetic curve discretized at the time-array $(t_1,\ldots,t_M)$ belonging to the wavelength interval λ_n; $a_{\nu_i,k}$ is the amplitude of k-th exponent with lifetime τ_k of CONTIN solution ν_i for i-th kinetic curve; $\overline{a}_{\nu_i,k}$ is the mean amplitude of the solutions, belonging to the same wavelength interval λ_n; and ε is the normalizing parameter. The first term in Eq. 3 is the aggregate error of solutions $[\nu]$, whereas the last term characterizes the smoothness of solutions calculated for neighboring wavelength values λ_i. The minimization of discrepancy function Eq. 3 was carried out by a Monte Carlo stochastic optimization method implemented in MATLAB (The MathWorks, Natick, MA). The value of normalizing parameter ε was changed iteratively to make the orders of magnitude of both terms in Eq. 3 equal to each other for the optimal solution $[\nu]$.

RESULTS

Energy transfer processes in PSI complexes isolated from the cyanobacterium *T. elongatus* were studied using pump-probe femtosecond spectroscopy. A comprehensive biochemical characterization of the purified PSI complexes is shown in Fig. 1. Isolated PSI complexes were purified using sucrose density gradient ultracentrifugation. Fig. 1 *A* shows SMA-PSI on the left and DM-PSI on the right. Liberated carotenoids can be seen as orange bands at the top of both sucrose gradients. The arrow indicates trimeric PSI, and DM-PSI migrates further into this gradient, presumably because of its more compact size, having lost the peripheral lipid anulus that is retained in SMA preparation. Although both methods preferentially extract trimeric PSI, SMA also shows larger supramolecular complexes that sediment to the bottom of the sucrose gradient (Fig. 1 *A*). The trimeric PSI was harvested from both sucrose gradients, buffer exchanged (to get rid of sucrose), and concentrated using centrifugal concentrators with 100 kDa cutoff. All downstream biochemical, biophysical, and spectroscopic studies were performed on these purified trimeric PSI complexes. Chlorophyll emission for SMA-PSI was shifted 2 nm to the red compared to DM-PSI (Fig. 1 *B*). This significant red shift suggests a more native orientation of the chlorophyll antenna within SMA-PSI (38). Absorption spectra across the UV-visible region show superimposable profiles between both extraction methods, with the exception of the absorbance maxima of the styrene at 220 nm (Fig. 1 *C*). BN-PAGE analysis reveals SMA-PSI is larger than DM-PSI, presumably because of increased thylakoid lipids retained within the native nanodisc (Fig. 1 *D*). The SDS-PAGE analysis in Fig. 1 *E* shows all key subunits are present in both preparations with some distinct differences. First, the bands in the 30–37 kDa range that are less prominent or missing altogether in the DM-PSI preparation have been previously identified as part of the NDH (NADH dehydrogenase) complex, which seems to be retained with SMA extraction (32). Also, the band at 14.4 kDa corresponds to PsaF, a peripherally associated subunit of unknown function in cyanobacteria, is significantly lost in SMA-PSI, with 18.6% of the PsaF remaining with the complex (Fig. 1 *E*). Stromal subunits C and E are very difficult to see because these subunits do not stain as prominently with silver; however, when the contrast is drastically decreased (data not shown), these subunits can be seen in both preparations.

The optical transitions in PSI complexes were induced by femtosecond pulses centered at 670 and 740 nm with pump energies of 20–40 and 100–200 nJ, respectively, which was

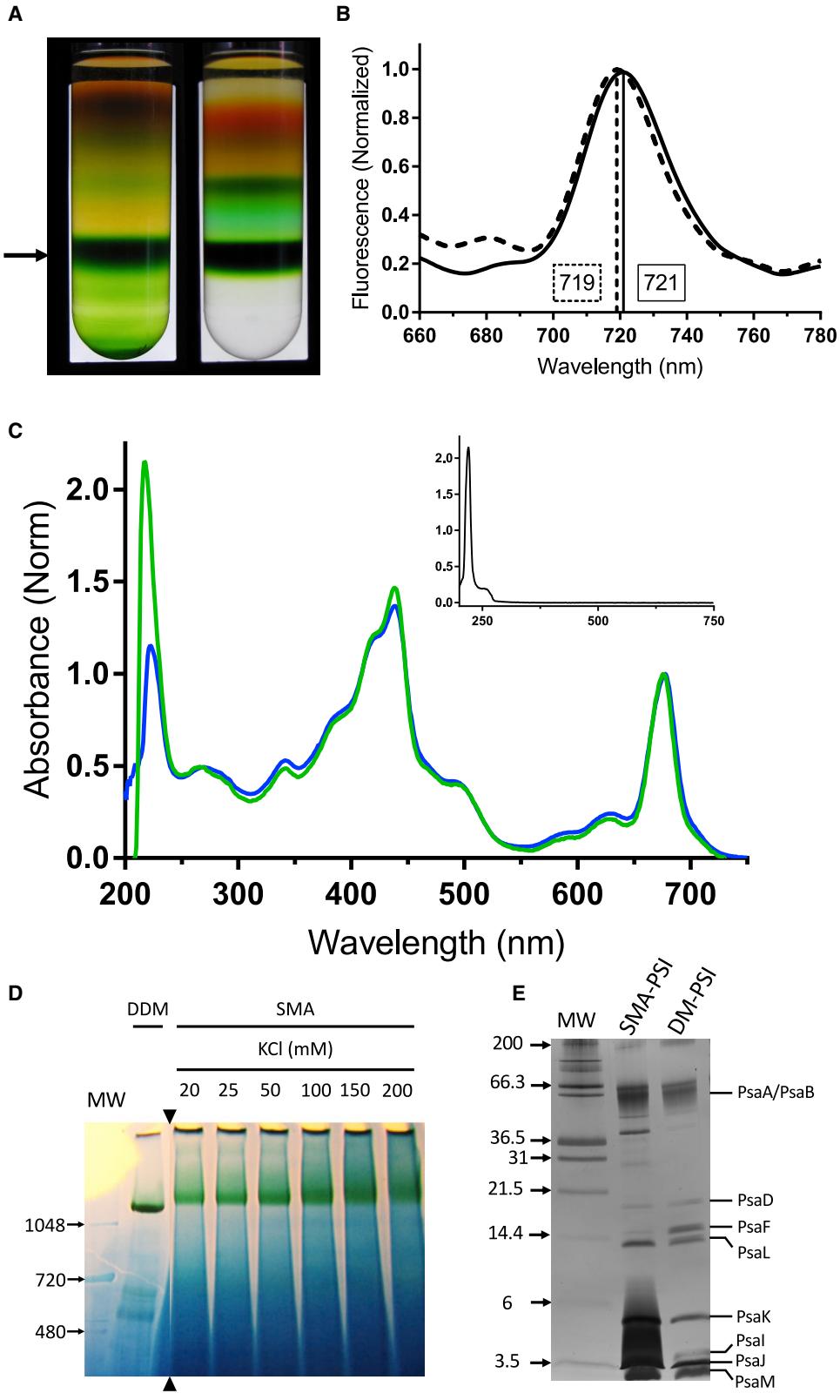

FIGURE 1 Biochemical characterization of the PSI RC extracted with DDM and SMA. (*A*) Sucrose density gradient ultracentrifugation gradients of supernatant after solubilization of thylakoid membranes with SMA (*left*) and DDM (*right*) are shown; the arrow indicates trimeric PSI for both preparations. (*B*) Chlorophyll fluorescence spectra of DM-PSI (*dotted*) and SMA-PSI (*solid*) are shown; wavelengths of fluorescence emission maxima are listed in boxes above the *x* axis. (*C*) UV-visible absorbance spectra of DM-PSI (*blue*) and SMA-PSI (*green*) are shown; absorbance of SMA 1440 copolymer is also shown (*inset*). (*D*) BN-PAGE analysis of DM-PSI and SMA-PSI is shown; black triangles indicate where the gel image was cropped, and all lanes were run on the same gel. The effect of increasing ionic strength on SMA extraction is also shown. (*E*) SDS-PAGE analysis of SMA-PSI and DDM-PSI is shown. (*D* and *E*) MW markers are shown in the first lane from left and are reported in kilodaltons (kDa). To see this figure in color, go online.

required to produce measurable optical changes. The time resolution at short delays was restricted by coherence spikes (see Materials and Methods). To avoid the contributions of coherent artifacts, the transient absorption changes at time delays <100 fs were ignored. Fig. 2 shows the transient spectra of PSI under conditions of specific excitation of

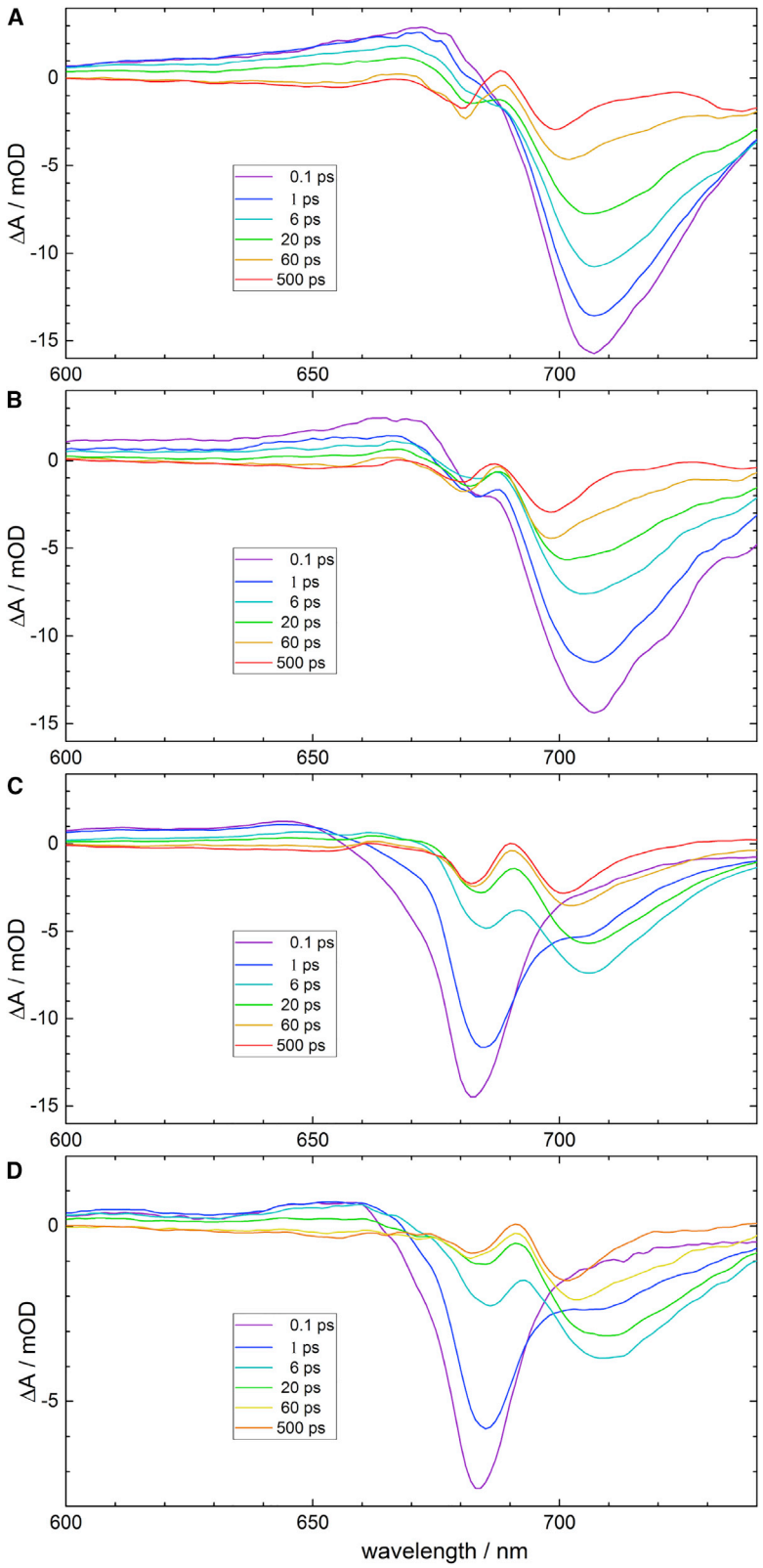

FIGURE 2 Transient absorption spectra of PSI at various delays (1–100 fs; 2–1 ps; 3–6 ps; 4–20 ps; 5–60 ps; 6–500 ps). 25 fs pump pulses were centered at 740 nm (*A* and *B*) and at 670 nm (*C* and *D*). DM-PSI (*A* and *C*) and SMA-PSI (*B* and *D*) complexes are shown. To see this figure in color, go online.

LWCs by femtosecond pulses at 740 nm (Fig. 2, *A* and *B*) and nonspecific excitation of the main part of the light-harvesting antenna by pulses at 670 nm (Fig. 2, *C* and *D*), respectively. The spectra of DM-PSI and SMA-PSI preparations are shown in Fig. 2, *A*–*D*, respectively. A common feature of the spectral changes induced by 740 nm pulses

at a minimal delay $t_d = 0.1$ ps is the presence of a broad bleaching band with a minimum at 708 nm and a wide positive-absorption region at 600–680 nm (Fig. 2, *A* and *B*). In the spectra of SMA-PSI samples at a time delay $t_d = 0.1$ ps, a feature is observed at 685 nm that is absent in DM-PSI preparations. The spectra obtained by excitation of PSI by 670 nm pulses at the delay $t_d = 0.1$ ps are characterized by a relatively narrow bleaching band with a minimum at 682 nm (Fig. 2, *C* and *D*). The spectral dynamics induced by 670 nm pulses looks very similar in the DM-PSI and SMA-PSI preparations. Recovery of the absorption spectra in this region occurs in the time domain of ~3 ps synchronously with the appearance of a bleaching band in the far-red region with a minimum at 706 nm (Fig. 2, *C* and *D*).

The transient spectra of DM- and SMA-PSI preparations induced by 740 nm excitation are combined for clarity on a single scale (Fig. 3). The transient spectra have unequal forms, which are distinguished by the bleaching at 680 nm present in SMA-PSI complexes at 0.1 ps delay and by a smaller magnitude of bleaching at 705 nm in these transients.

The transient absorption changes in the DM-PSI and SMA-PSI preparations at the indicative wavelength of 680 nm are plotted in Fig. 4 by black and red traces, respectively. The positive absorbance at 100 fs in DM-PSI preparations could be attributed to the excited state of Chl *a* (39), whereas the bleach at 680 nm in SMA-PSI preparations could be due to the ground state depletion of primary electron acceptor (40). The decay kinetics at delays $t_d \leq 120$ fs may be affected by the coherent artifacts (Fig. S1). The two-exponential fitting gave the lifetimes $\tau_1 = 0.64$ ps, $\tau_2 = 23.9$ ps for DM-PSI and $\tau_1 = 1.4$ ps, $\tau_2 = 21.7$ ps for SMA-PSI preparations, respectively. Fig. 4 provides evidence of an ultrafast ($\lesssim$100 fs) bleaching at 680 nm in the SMA-PSI preparations, which is indicative of the ion-radical pair $P_{700}^{+}A_0^{-}$ formation in these complexes.

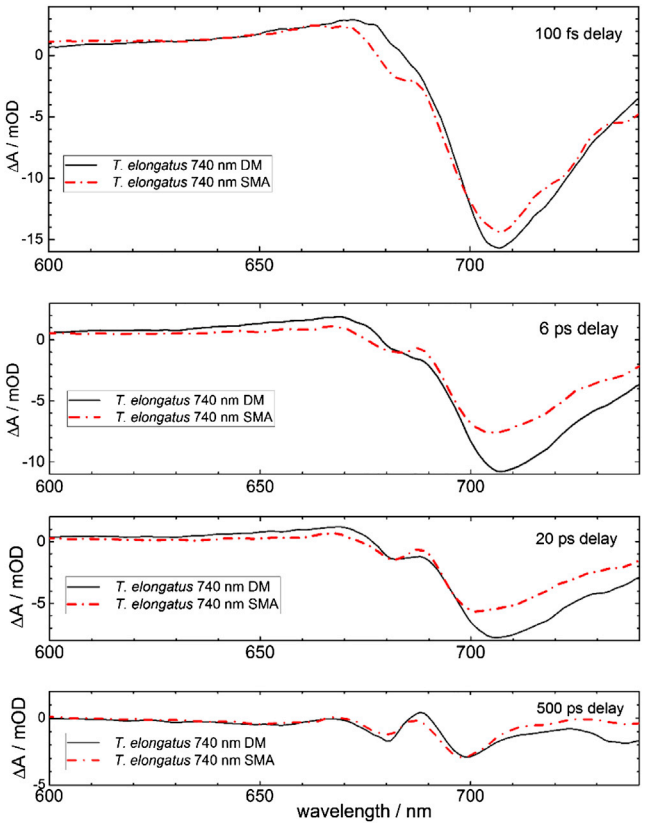

FIGURE 3 Transient absorption spectra of PSI at various delays (1–100 fs; 2–6 ps; 3–20 ps; 4–500 ps). DM-PSI (*black solid*) or SMA-PSI (*red dashed-dotted*) complexes excited by 740 nm pulses are shown. To see this figure in color, go online.

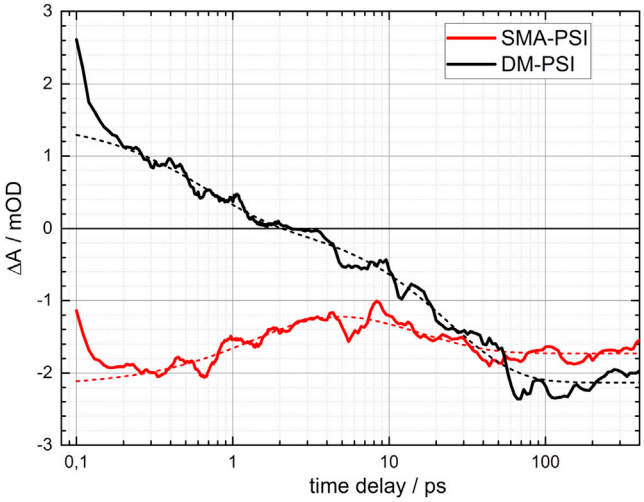

FIGURE 4 Transient absorption changes in the DM-PSI (*black*) and SMA-PSI (*red*) samples at the probe wavelength 680 nm upon excitation by pulses centered at 740 nm (the energy of 200 nJ). The dashed traces were obtained by multiexponential fitting with lifetimes $\tau_1 = 0.64$ ps, $\tau_2 = 23.9$ ps (DM-PSI), and $\tau_1 = 1.6$ ps, $\tau_2 = 16.8$ ps (SMA-PSI). To see this figure in color, go online.

The final spectra of both samples at the maximal delay $t_d = 500$ ps (Figs. 3 and S2) have a common characteristic signature with the two minima at 680 and 700 nm; its nature will be discussed in detail later. The spectrum of DM-PSI preparation has a butterfly-shaped feature in the 470–520 nm region that is absent in the SMA-PSI preparation (Fig. S2). This feature was assigned to a local electrochromic shift of carotenoid molecule localized in the vicinity of the anion A_1^{-} (41).

To make a deconvolution of the observed transition spectra into kinetic components, a global numerical analysis of spectral matrices of the form $\Delta A(\lambda, t)$ was performed in the spectral range of 430–720 nm and in the time interval of 0.05–500 ps. It was assumed that the spectral changes are the sum of three exponential components and offset, as described by the following equation:

$$\Delta A(\lambda, t) = \sum_{i=1,2,3} \Delta A_i(\lambda) \times \exp(-k_i t) + \Delta A_0(\lambda). \quad (4)$$

Thus, the global approximating model included four spectral components (three exponents and a stationary

spectrum at large delay) and three kinetic parameters k_1, k_2, and k_3, the values of which were obtained by nonlinear optimization. For given values of k_1, k_2, and k_3, the components $\Delta A_i(\lambda)$ were calculated by solving the linear least squares regression problem following the standard methods of data regression (42).

Fig. 5 *A* shows the results of the global exponential deconvolution of the spectral dynamics of DM-PSI preparations from *T. elongatus* upon direct excitation of LWC by a pulse at 740 nm. In this regard, the positive amplitude of the spectrum corresponds to an increase in bleaching in this optical region and the negative one to an increase of the optical absorption. Under long-wavelength excitation, the optical dynamics of PSI revealed an ultrafast component with characteristic time $\tau_1 = 80$ fs, which may originate from nonlinear coherent artifacts (see Fig. S1), so it is not included in Fig. 5 *A*. The second component, with $\tau_2 = 2.4$ ps, has a small amplitude and nearly symmetrical form: the bleach decrease at 705 nm $\Delta A_{705} = +2.8$ mOD and the absorption decrease at 685 nm $\Delta A_{685} = -1.8$ mOD. The contribution of this component to the energy-trapping processes LWC → RC → $P_{700}{}^{(+)}A_0{}^{(-)}$ seems unlikely because the energy trapping by charge separation reactions is accompanied by essentially asymmetrical absorbance changes: the considerable decrease of LWC bleaching ($\Delta A_{705} = +14$ mOD) and order-of-magnitude smaller changes at 685 nm ($\Delta A_{685} \approx -2$ mOD; see Fig. 2 *A*). The component with $\tau_2 = 2.4$ ps may arise from fast energy redistribution processes between LWC and the antenna pigments, which proceed in the time range of a few picoseconds (19). The estimate of the energy distribution rate constant k_1 (Scheme 1) is given below. The main spectral changes caused by 740 nm excitation of DM-PSI preparations occurred with a characteristic time $\tau_3 = 36$ ps, which characterizes the process of energy transfer from the LWC forms in antennae to the cofactors in RCs. Note that because the characteristic time of electron transfer from chlorophyll A_0 to phylloquinone A_1 is ~25 ps (2), the kinetics of the intermediate reduction of chlorophyll A_0 remains unresolved. Consequently, spectral changes in the absorption maximum of A_0 (685 nm) at $\tau \geq 36$ ps are absent (Figs. 2 *A* and 5 *A*); the spectrum at the maximal delay $t_d = 500$ ps reflects the spectrum of the ion-radical pair $P_{700}{}^{+}A_1{}^{-}$ (43).

The exponential deconvolution of the spectral dynamics in SMA-PSI complexes excited by a similar long-wave pulse (740 nm) is shown in Fig. 5 *B*. Qualitatively, the optical dynamics in these preparations resembled the dynamics of DM-PSI samples (Fig. 5 *A*); however, two significant differences were revealed. First, the fast component $\tau_2 = 2.5$ ps in SMA-PSI preparations has an approximately doubled amplitude relative to DM-PSI and reveals an additional minimum at 685 nm, which can be attributed to the chlorophyll A_0 absorption (2). Secondly, the amplitude of the slow component $\tau_3 = 37$ ps is strongly reduced relative to the final spectrum of the radical-ion pair $P_{700}{}^{+}A_1{}^{-}$. All these features together indicate that in SMA-PSI preparation, a fast energy transfer from the LWC forms to the RC is observed.

Fig. 5 *C* shows the deconvolution of the spectral dynamics of DM-PSI excited by pulses at 670 nm, which required three exponential components with the characteristic times $\tau_1 = 0.52$ ps, $\tau_2 = 2.7$ ps, and $\tau_3 = 36$ ps, respectively, as well as the final differential spectrum of the ion-radical pair $P_{700}{}^{+}A_1{}^{-}$ (*offset*). Similar decay-associated spectra were obtained for SMA-PSI (Fig. 5 *D*). Components with $\tau_1 = 0.5$–0.6 ps and $\tau_2 = 2.7$–3.2 ps characterize the process of energy transfer from excited chlorophyll molecules with an absorption maximum at ~670 nm to longer wavelengths with a maximum at ~710 nm. The slowest component ($\tau_3 = 36$ ps) describes the process of energy transfer from the LWC to the PSI RC and the subsequent charge separation process with the formation of the final spectrum of the ion-radical pair $P_{700}{}^{+}A_1{}^{-}$. Notably, the relative amplitude of the component $\tau_3 = 36$ ps in PSI preparations excited by pulses at 670 nm is smaller than the amplitude of the analogous component observed when the LWCs were excited directly by pulses at 740 nm (Fig. 5 *A*). Apparently, this difference is due to the fact that when PSI is excited by 670 nm pulses, a significant part of the energy flows from the light-harvesting antenna directly to the RC, bypassing the LWCs. The relative contributions of both energy transfer channels can be estimated by comparing the amplitude of the LWC bleaching in the $\tau_3 = 36$ ps component at 710 nm (ΔA_{LWC}) with the amplitude of P_{700} bleaching in the final $P_{700}{}^{+}A_1{}^{-}$ spectrum at 700 nm (ΔA_{P700}). Upon excitation of the DM-PSI preparation by pulses at 740 nm, all energy is localized on the LWC forms, and the ratio $\Delta A_{LWC}/\Delta A_{P700} = 3.0$. When PSI is excited by pulses at 670 nm, the ratio $\Delta A_{LWC}/\Delta A_{P700} = 2.5$, so 17% of the energy flows directly into the RC, and 83% is redistributed to the LWCs. It is noteworthy that in the SMA-PSI samples excited by 740 nm pulses, the ratio $\Delta A_{LWC}/\Delta A_{P700} = 1.7$; hence, ~45% of the energy gets the RC with ultrafast femtosecond kinetics on the timescale of 0.1 ps (Figs. 3 and 4).

In summary, the energy trapping in DM-PSI and SMA-PSI preparations demonstrates a marked difference. In the DM-PSI sample, the energy trapping upon 740 nm excitation proceeded mainly at 36 ps (Fig. 5 *A*), and the fast symmetric 2.4 ps component was assigned to processes of energy redistribution in the antenna. In the SMA-PSI sample, an ultrafast ($t_d \leq 0.1$ ps) bleaching of the primary electron acceptor A_0 was revealed in ~45% of complexes (Fig. 5 *B*). A transient increase of absorption at 680 nm was observed in these centers at the time range of 1–5 ps (Fig. 4, *red*), which finds expression in the asymmetric shape of the 2.5 ps decay-associated spectrum (Fig. 5 *B*, *blue*). This absorption increase may reflect fast Stokes shifts caused by formation of the ion-radical pair $P_{700}{}^{(+)}A_0{}^{(-)}$.

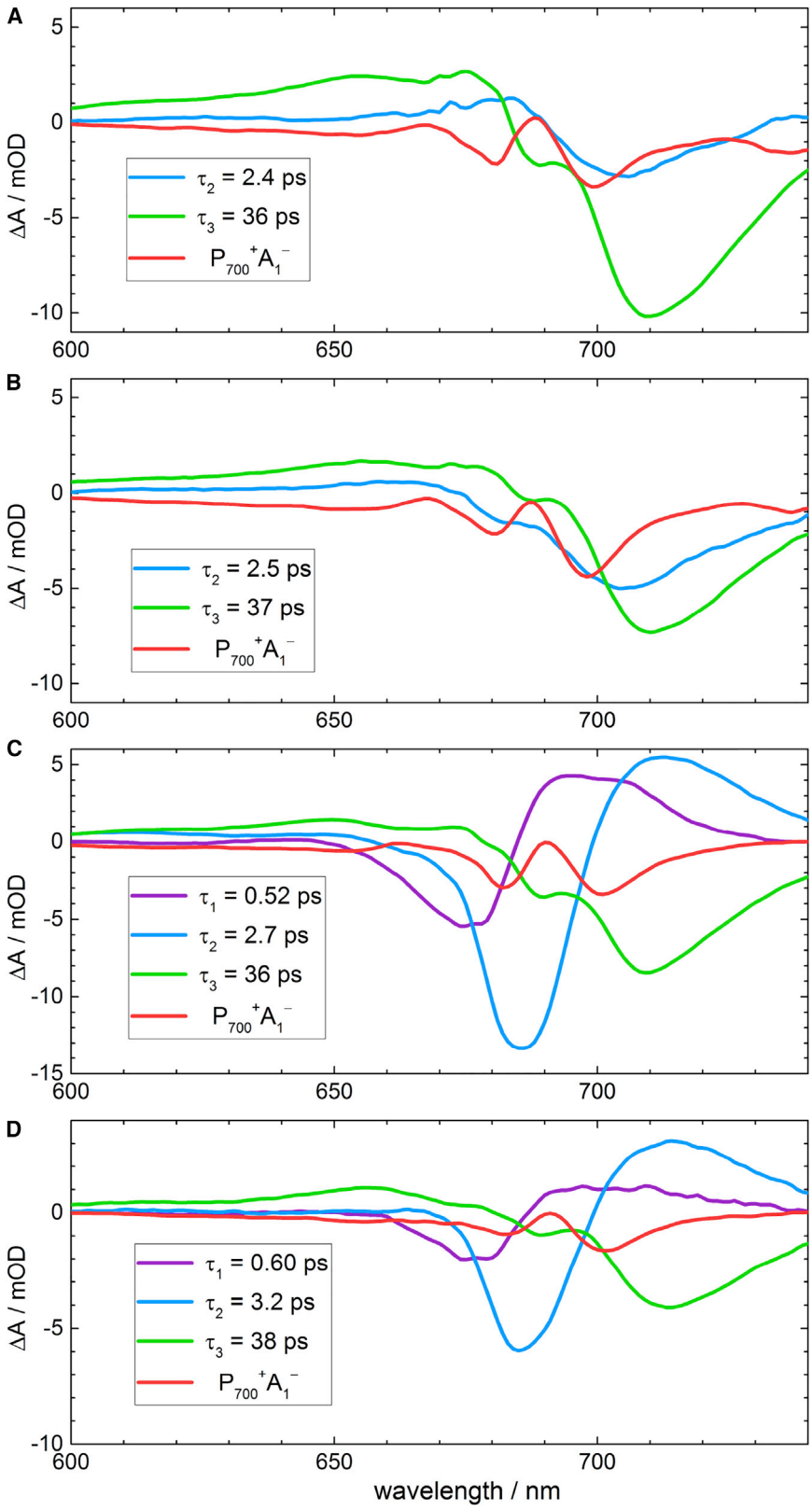

FIGURE 5 Exponential deconvolution of the transient spectral dynamics in PSI preparations from *T. elongatus* excited by pulses at 740 nm (*A* and *B*) and 670 nm (*C* and *D*). DM-PSI (*A* and *C*) or SMA-PSI (*B* and *D*) complexes are shown. To see this figure in color, go online.

An important goal in determining the mechanisms of energy transfer and charge separation in PSI is to find specific markers to reveal individual intermediates in these processes. The data shown in Figs. 2, 3, and 5 allow us to conclude that the formation of the P_{700}^+ cation is characterized by a red electrochromic shift of the absorption band of the nearest second chlorophyll pair Chl2A/Chl2B with an absorption maximum of ~685 nm. Because the spectral dynamics in DM-PSI complexes excited by femtosecond pulses at 740 nm does not contain a discernible bleaching band at 685 nm, the classical electrochromic butterfly shape is clearly expressed in the spectral component $\tau_3 = 38$ ps and in the stationary spectrum of the final radical ion-pair $P_{700}^+A_1^-$ (Fig. 5, *green* and *red lines*). The deconvolution of $P_{700}^+A_1^-$ spectrum into the bleaching band (λ = 697.0 nm, σ = 8.0 nm) and the electrochromic shift of the band ($\lambda = 682.7 \rightarrow 690.0$ nm, $\sigma = 5.2$ nm) describes almost exactly the experimental spectrum of $P_{700}^+A_1^-$ (Fig. 6).

The magnitude of the electrochromic pattern of P_{700}^+ in the region of 680–700 nm $\chi(t)$ can be determined from the second derivative of the spectra as explained in Fig. S3; its dynamics for DM-PSI and SMA-PSI preparations is shown in Fig. 7 by blue and red traces, respectively. The comparison of two samples demonstrates that in the DM-PSI preparation, formation of the P_{700}^+ electrochromic signature takes place to a great extent on the timescale of 40 ps (Fig. 7), whereas in the SMA-PSI preparation, an ultrafast ($\leq$0.1 ps) formation of the cationic state P_{700}^+ takes place in a large part of the complexes (Fig. 7).

To visualize the processes of energy migration in the antenna and charge separation in the RC in more detail, the spectral changes in the DM-PSI and SMA-PSI preparations were analyzed in the time interval of 0.1–500 ps by using the CONTIN program, which employs the inverse Laplace transform method for a multiexponential deconvolution of the kinetics (37). The data obtained are shown in Fig. 8 in the form of two-dimensional spectrograms. Areas in which spectral dynamics are absent are marked in green, areas with optical bleaching in blue, and areas in which an increase in the optical absorption of the samples was revealed in red. Fig. 8 *A* demonstrates the map of spectral changes in the DM-PSI complexes excited in far red (740 nm). The spectrogram confirms the results of global exponential deconvolution presented in Fig. 5 *A*, in which the two exponential components are found out, with the main changes (bleaching at 678 nm and absorption recovering at 710 nm) occurred at ~40 ps. The analogous spectral changes in the SMA-PSI complexes are shown in Fig. 8 *B*. The main difference with the DM-PSI samples are the appearance of an ultrafast bleaching at ~680 nm (compare with Fig. 4) and the reciprocal decrease in the magnitude of the slow 40 ps component attributed to the energy transfer from the LWC to RC. Fig. 8 *C* shows the excitation migration from pigments absorbing at 670 nm to the LWC in the DM-PSI complexes excited at 670 nm. The excitation migration looks like a consecutive process, in which the energy is transferred step by step from the high-energy to low-energy chlorophyll forms. The charge separation occurs predominantly at 40 ps, similar to the case of direct far-red excitation at 740 nm (Fig. 5 *A*).

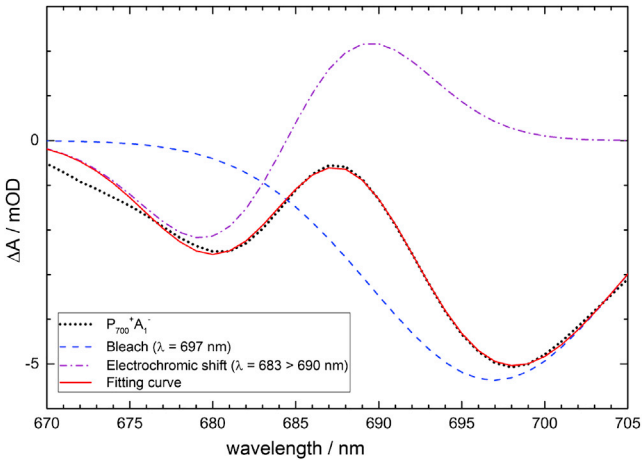

FIGURE 6 The deconvolution of the differential spectrum of the ion-radical state of $P_{700}^+A_1^-$ into two components: bleaching (λ = 697.0 nm, σ = 8.0 nm, *dashed*) and electrochromic shift ($\lambda = 682.7 \rightarrow$ 690.0 nm, σ = 5.2 nm, *dash-dotted*). The experimental data are taken from Fig. 2 *B* for SMA-PSI sample (*dots*), and the model curve (*solid*) is the sum of the two contributions. To see this figure in color, go online.

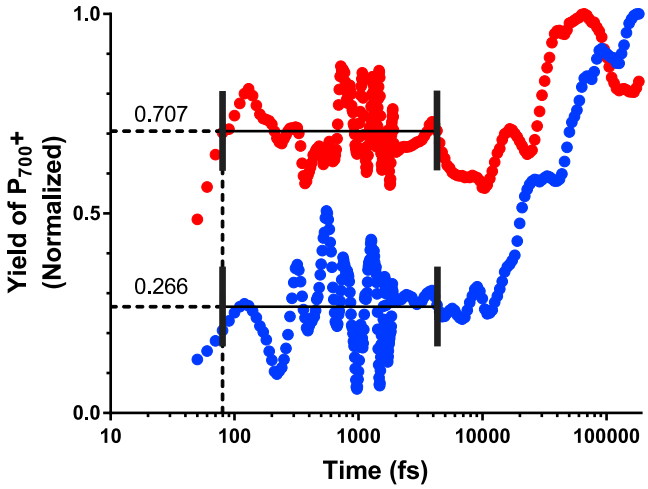

FIGURE 7 The contribution $\chi(t)$ of the ionic state P_{700}^+ to the transient spectra $\Delta A(\lambda, t)$ of DM-PSI (*blue*) and SMA-PSI (*red*) complexes from *T. elongatus* excited by a long-wave pulse of 740 nm (see Fig. S3 for details). The solid lines indicate the average between the vertical bars. Dotted lines are extrapolations back to *x* and *y* axes. The numerical values correspond to the ratio of P_{700}^+ produced in the timescale of 0.1–5 ps. To see this figure in color, go online.

DISCUSSION

The current literature continues to dispute the nature of the primary and secondary donors and electron acceptors in PSI, as well as the limiting step of the process of converting solar

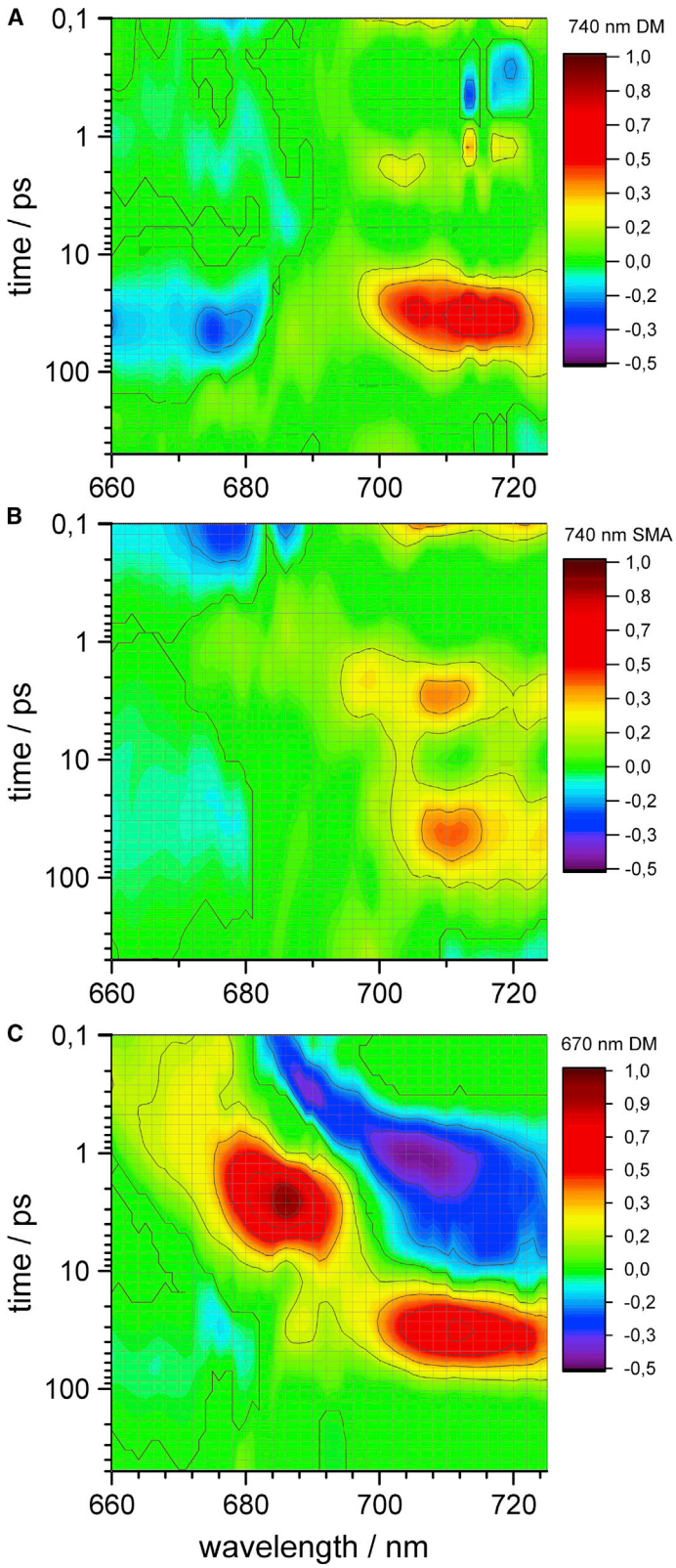

FIGURE 8 Spectrograms of the distribution of the kinetic exponential components in the region of the chlorophyll Q_Y absorption band, obtained using the CONTIN program for PSI from cyanobacterium *T. elongatus*. The maximal excitation pulse at 740 nm (*A* and *B*) and 670 nm (*C*) is shown. DM-PSI (*A* and *C*) and SMA-PSI (*B*) preparations are shown. The scale of the amplitudes of the components is shown to the right of the spectrograms. To see this figure in color, go online.

energy in protein complexes. The complexity of the problem is due to the fact that in PSI, it is impossible to separate the chlorophylls of the light-harvesting antenna from electron-transfer cofactors in the RC without disturbing the overall structure of the complex. The energy transfer in the antenna and charge separation in the RC occurs on the timescale of

10^{-13}–10^{-11} s (2,4,5,44–46). The spectral and temporal intersections of these processes result in appearance of controversial suggestions on the mechanism of primary steps of energy conversion in PSI. In particular, there is no single point of view on the nature of the primary donor and electron acceptor in PSI, and several alternative mechanisms for the generation of primary ion-radical states are considered.

According to the most common opinion, photoinduced charge separation is preceded by the formation of an excited state of a special pair, P_{700}*. The P_{700}* state can be formed either directly, as a result of the absorption of a quantum of light by the P_{700} dimer (*channel (1)* in Scheme 1), or indirectly, as a result of the transfer of energy from the antenna (*channels (2)* and *(3)* in Scheme 1). In doing so, the energy transfer in the antenna occurs in the time interval of several picoseconds (47); a close time of 1.5–3 ps was attributed to the initial reaction of electron transport by most authors (2). A mechanism, according to which the charge separation occurs between the Chl2/Chl3 chlorophylls of the A_0 heterodimer, has been actively discussed (7,48,49). Results of pump-probe femtosecond spectroscopy with excitation of PSI complexes in the far-red region demonstrated the formation of a signal for the primary ion-radical pair of $P_{700}^{+}A_0^{-}$ already at a delay of 100 fs (4,9). The method of two-dimensional femtosecond spectroscopy was used to study the energy transfer processes in PSI, which revealed the presence of fast (2–4 ps) energy transfer to LWCs (5).

The results obtained in this work by the femtosecond pump to supercontinuum probe technique of *T. elongatus* DM-PSI preparations are similar to the data obtained for PSI complexes from the strain *C. thermalis* PCC 7203 grown under white light, i.e., without synthesis of LWC *f* (6). Spectrally unresolvable bleaching at 710 nm and excited state absorption in the 620–670 nm region were observed in both cases when samples were excited in the far-red region (compare Fig. 2 *A* of this work and Fig. 3 *B* of Kaucikas et al. (6)). Absorption recovery of the LWC in antenna and the formation of the final spectrum of the ion-radical pair $P_{700}^{+}A_1^{-}$ occurred with a characteristic time of 36 ps (Fig. 8 *A* of this work and Fig. 6 *B* of Kaucikas et al. (6)). However, the rate of energy transfer to LWC when the antenna is excited by pulses at 670 nm was very different in these two strains: in the *T. elongatus,* energy transfer occurred in the 0.2–2 ps time domain with the main time $\tau_2 = 2.7$ ps (Figs. 5 *C* and 8 *C*), whereas in the *C. thermalis* PCC 7203, this process was carried out with a time of ~20 ps (Fig. 6 *A* and Fig. 9 *A* of Kaucikas et al. (6)), getting into the same time interval with energy transfer processes from the LWCs to the RC and the formation of the final ion-radical pair $P_{700}^{+}A_1^{-}$.

Thus, in DM-PSI complexes, excitation energy was transferred to the RC with a time of ~36 ps, regardless of whether excitation occurred in the far-red region or at the maximum of the antenna's absorption at 670 nm. A close time of 16–19 ps was obtained using two-dimensional electronic spectroscopy for energy transfer to the RC of the strains of *Synechococcus* sp. PCC 7002 and *Synechocystis* sp. PCC 6803 (5).

We attempt to estimate the rate constants and relative extents of energy transfer processes induced by 670 nm excitation (Scheme 1). We assume that the reactions of forward energy migration from An* to LWC (k_1) and to RC (k_2) in DM-PSI from *T. elongatus* are two concurrent processes. The last process was observed with a quantum yield of 17% in the given experiments, and 83% of the excitation was redistributed to the LWC. The observable lifetime of overall process $\tau_2 = 1/(k_1 + k_2)$ is 2.7 ps. The quantum yield of the LWC excitation is 83%, so the ratio of the rate constants $k_1/k_2 = 0.83/0.17$. We thereby get $k_1 = 3.1 \times 10^{11}$ s^{-1} and $k_2 = 6.3 \times 10^{10}$ s^{-1}. The rate constant of backward energy transfer from LWC to RC is $k_3 = 1/\tau_3 = 2.8 \times 10^{10}$ s^{-1}. Unfortunately, the relative extents of these reactions could not be determined precisely, several factors making such a determination difficult. First, the RC comprises only six chlorophyll molecules, whereas the antenna includes 90 chlorophylls; this gives rise to an ineluctable high noise level. Second, the six chlorophyll molecules in the RC are strongly coupled in a combined electronic system (50,51), and their quantitative spectral analysis is rather challenging. Third, the transient spectra obtained by pump-probe femtosecond spectroscopy represents a mixture of ground state bleaching (always negative), excited state absorption (always positive), and stimulated emission (always negative). These spectral components have comparable amplitudes in the range of chlorophyll Q_Y band absorption.

The spectrum of the radical ion pair $P_{700}^{+}A_1^{-}$ was observed at delays $\geq$50 ps. This spectrum can be considered as a superposition of P_{700} bleaching at ~700 nm and the electrochromic band shift of A_0 at ~685 nm (52). In the SMA-PSI preparation, the bleaching band has the maximum at $\lambda = 697.0$ nm and the Gaussian root mean-square (RMS) width $\sigma = 8.0$ nm, whereas the electrochromic shift has the band parameters $\lambda = 682.7 \rightarrow 690.0$ nm, $\sigma = 5.2$ nm. The typical RMS width of chlorophyll is 6.3 nm (53). An RMS width of 6.5 nm has been determined by hole-burning experiments for P_{700} using PSI complexes from spinach at 1.6 K (54). Taking into account the band broadening at high temperature, the estimation $\sigma = 8.0$ nm seems to be consistent with these measurements.

The electrochromic shift of Q_Y band at 685 nm in the $P_{700}^{+}A_1^{-}$ state of DM-PSI preparation is twofold larger than in the SMA-PSI samples (Fig. S4). In consequence of this fact, the difference between the SMA- and DM-PSI preparations is especially noticeable in the region of the carotenoid absorption at 470–520 nm, in which the SMA-PSI preparation does not reveal electrochromic features. A high variability of the carotenoid band shift at 480 nm upon charging of the A_{1A} and A_{1B} sites was observed in

various PSI preparations both in solution and in trehalose glass (55). The increase of electrochromic effects in the DM-PSI preparation could be explained in two different ways. On the one hand, the enhanced electrochromism in the presence of detergent can be caused by a significant conformational rearrangement significantly changing the geometry of the pigment-protein complex, both near P_{700} and A_1 sites. More plausibly, the magnitude of electrochromic bandshift, which depends on the dielectric permittivity of the protein-water interface (52), was sufficiently lowered by DM solubilization. The detergent forms a nonpolar layer around the PSI complex, expelling water molecules from cavities on the protein surface. In the second case, the enhanced electrochromism will be a combined result of several factors decreasing dielectric permittivity of the DM-PSI preparation, such as the low concentration of water at the surface, the intercalation of detergent into the pigment-protein complex, and the decreased conformational mobility of chargeable amino acid groups at the protein surface.

The main results of this work clearly demonstrate that the use of DM detergent significantly affects the rate and efficiency of energy transfer processes initiated by the excitation of LWCs in PSI. In SMA-PSI complexes excited at 740 nm, the ultrafast bleaching at 680 nm (Fig. 4) and the electrochromic feature at 680–690 nm (Fig. 7) suggest an ultrafast formation of the ion-radical state $P_{700}{}^{+}A_0{}^{-}$ in the time interval of $\leq$0.1 ps. This means that the excited state $(P_{700}A_0)^*$ can be directly produced by far-red pulses and initiates the primary photochemistry via the first channel in Scheme 1; the respective rate constant of the primary charge separation m_1 is as high as 10 ps^{-1}. In these preparations excited in the far-red region of the antenna (740 nm), ~45% of the energy reached the RC with a characteristic time of $\leq$100 fs (Figs. 4 and 7). In ~55% of the complexes, the excitation remained localized on the LWCs, and the transfer of excitation energy to the RC occurred with the characteristic time of 36 ps. In contrast, in DM-PSI complexes excited at 740 nm, the bleaching at 680 nm (Fig. 4) and the electrochromic shift at 680–690 nm (Fig. 7) developed at the timescale of ~10 ps. These findings may help to specify the primary events in the PSI photochemistry.

The substantiation of Chl2 as a primary electron donor was supported by the observation in PSI from *Chlamydomonas reinhardtii* excited at 700 nm of a bleaching band at ~680 nm, which appeared with a characteristic time of 6–9 ps and was assigned to the transition Chl2* → $Chl2^{+}Chl3^{-}$ (48,56). In agreement with these observations, the transient bleaching at 680 nm was observed in DM-PSI preparation excited at 740 nm, and the kinetics was nonexponential and had an effective time of ~10 ps (Fig. 4, *black*). In contrast to this, in SMA-PSI complexes excited in the far-red region, a bleaching at 680 nm was seen already at 0.1 ps (Figs. 2 *B*, 3 *B*, and 4, *red*), in line with the dynamics of PSI from *Synechocystis* sp. PCC 6803 excited at 720–760 nm (4,9). It is noteworthy that the PSI from *Synechocystis* sp. PCC 6803 does not contain LWC forms absorbing in the 720–760 nm region (57). Because the absorption band of the Chl2/Chl3 heterodimer is centered at ~686 nm (40,52), the 740 nm pulses in our measurements with SMA-PSI complexes did not overlap with the Q_Y band of Chl2/Chl3 heterodimer but excited either the LWC in antenna (~55%) or P_{700} directly in the far-red tail of its absorption spectrum (~45%). Thus, these results corroborate an ultrafast formation of the ion-radical pair $P_{700}{}^{+}A_0{}^{-}$ as the primary charge-separated state in PSI from *T. elongatus*.

An ultrafast charge separation in PSI may proceed because of strong electronic coupling between P_{700} and the nearest Chl2 (50), analogous to the intradimer electron transfer observed in synthetic chlorophyll analogs (τ = 170 fs) (58). High-pressure hole-burning spectroscopy revealed for red pigment pools in the PSI core a conformational mixing between the locally excited and charge transfer configurations that can be considered as typical excimers (59). The PSI absorption spectrum in the red edge demonstrates an exponential dependence (known as the Urbach rule), which was attributed to the effect of strong electronic coupling between the excited P_{700}* and the charge-separated states $P_{700}{}^{+}A_{0A}{}^{-}$ and $P_{700}{}^{+}A_{0B}{}^{-}$ in both branches of redox cofactors (4). The ultrafast channel of charge separation is indicated in Scheme 1 by the rate constant m_1.

A very slow charge separation was observed in PSI complexes from *T. elongatus* at liquid helium temperatures under illumination with far-red light at 754–808 nm (17). Because an uphill energy transfer is unrealizable at such temperatures, a direct activationless transition from excited LWC in antenna to a CT state in RC via a superexchange mechanism was proposed (17). A similar mechanism was considered for the LH1-RC system of purple bacteria (18). The possibility of such direct transition may be due to a strong electron-phonon coupling in PSI (59,60), which makes conditions for a mixing of neutral exciton and polar charge transfer states (excimer). This slow, direct transition from excited LWC to a charge-separated state in the RC is denoted by the rate constant m_0 in Scheme 1.

At ambient temperature, energy transfer from excited LWCs in antennae to the RC apparently proceeds via the excited state P_{700}* at the timescale of 20–100 ps (5,6). This intermediate channel of charge separation is controlled by the uphill transition marked by the rate constant k_3 in Scheme 1. Because of the presence of LWC C-719 in the antenna of *T. elongatus*, the far-red pulse (740 nm) excited almost in equal proportions both the LWC in antenna and the dimer P_{700} in RC of the SMA-PSI complex, so channels (1) and (2) provided comparable contributions to the PSI photochemistry. In the DM-PSI preparation, only channel (2) was observed; the low quantum yield of direct P_{700} excitation may be the result of a reduced electronic coupling caused by the presence of detergent.

The nonspecific excitation of the main part of light-harvesting antenna chlorophyll by femtosecond pulses at 670 nm induces a sequence of energy transfer processes from high-energy forms of chlorophyll with an absorption maximum of ~670 nm to longer wavelengths with a maximum of ~710 nm. In the sequence of these reactions, two exponential components can be distinguished with times $\tau_1 = 0.56$ ps and $\tau_2 = 2.8$ ps.

Thus, in this work, we were able to demonstrate a difference in the femtosecond kinetics of electron transfer from two different preparations of a cyanobacterial PSI. Although the spectral properties of these two complexes are quite similar, the kinetics of the first step in electron transfer reveals a new, ultrafast component that, to our knowledge, has never been observed in the detergent-solubilized forms of PSI from the commonly studied cyanobacterium *T. elongatus*. The distinct differences that enable this much faster electron transfer are not known but may suggest some structural change occurs in the protein environment of these cofactors during detergent isolation. Further investigation will be needed to compare the details of how the cofactors are bound within this nondetergent form of PSI.

SUPPORTING MATERIAL

Supporting Material can be found online at https://doi.org/10.1016/j.bpj.2019.11.3391.

AUTHOR CONTRIBUTIONS

Experimental design was conceived by D.A.C., M.D.M., V.A.N., and B.D.B.; *Thermosynechococcus elongatus* was grown by J.N.; PSI extractions were performed by N.G.B.; biochemical characterization of PSI-SMALP (styrene maleic acid lipid particle) was performed by N.G.B. and B.D.B.; the spectroscopy was performed by I.V.S., F.E.G., and M.D.M.; this manuscript was written by D.A.C., N.G.B., and B.D.B.

ACKNOWLEDGMENTS

This work was supported by the Russian Science Foundation (Grant RSF 19-14-00366). Support for B.D.B. has been provided from the Gibson Family Foundation, the Dr. Donald L. Akers Faculty Enrichment Fellowship, and National Science Foundation (DGE- 0801470 and EPS-1004083). N.G.B. and B.D.B. have been supported via a Joint Directed Research Development Award from University of Tennessee at Knoxville/Oak Ridge National Laboratory Science Alliance to B.D.B. N.G.B. has also been supported via a Penley Fellowship.

REFERENCES

1. Jordan, P., P. Fromme, …, N. Krauss. 2001. Three-dimensional structure of cyanobacterial photosystem I at 2.5 A resolution. *Nature.* 411:909–917.
2. Savikhin, S., and R. Jankowiak. 2014. Mechanism of primary charge separation in photosynthetic reaction centers. *In* The Biophysics of Photosynthesis. J. Golbeck and A. van der Est, eds. Springer, pp. 193–240.
3. Reimers, J. R., M. Biczysko, …, E. Krausz. 2016. Challenges facing an understanding of the nature of low-energy excited states in photosynthesis. *Biochim. Biophys. Acta.* 1857:1627–1640.
4. Cherepanov, D. A., I. V. Shelaev, …, V. A. Nadtochenko. 2017. Mechanism of adiabatic primary electron transfer in photosystem I: Femtosecond spectroscopy upon excitation of reaction center in the far-red edge of the QY band. *Biochim. Biophys. Acta Bioenerg.* 1858:895–905.
5. Lee, Y., M. Gorka, …, J. M. Anna. 2018. Ultrafast energy transfer involving the red chlorophylls of cyanobacterial photosystem I probed through two-dimensional electronic spectroscopy. *J. Am. Chem. Soc.* 140:11631–11638.
6. Kaucikas, M., D. Nürnberg, …, J. J. van Thor. 2017. Femtosecond visible transient absorption spectroscopy of chlorophyll f-containing photosystem I. *Biophys. J.* 112:234–249.
7. Holzwarth, A. R., M. G. Müller, …, W. Lubitz. 2006. Ultrafast transient absorption studies on photosystem I reaction centers from Chlamydomonas reinhardtii. 2: mutations near the P700 reaction center chlorophylls provide new insight into the nature of the primary electron donor. *Biophys. J.* 90:552–565.
8. Srinivasan, N., and J. H. Golbeck. 2009. Protein-cofactor interactions in bioenergetic complexes: the role of the A1A and A1B phylloquinones in Photosystem I. *Biochim. Biophys. Acta.* 1787:1057–1088.
9. Shelaev, I. V., F. E. Gostev, …, A. Y. Semenov. 2010. Femtosecond primary charge separation in Synechocystis sp. PCC 6803 photosystem I. *Biochim. Biophys. Acta.* 1797:1410–1420.
10. Di Donato, M., A. D. Stahl, …, M. L. Groot. 2011. Cofactors involved in light-driven charge separation in photosystem I identified by subpicosecond infrared spectroscopy. *Biochemistry.* 50:480–490.
11. Zamzam, N., M. Kaucikas, …, J. J. van Thor. 2019. Femtosecond infrared spectroscopy of chlorophyll f-containing photosystem I. *Phys. Chem. Chem. Phys.* 21:1224–1234.
12. Brettel, K., and W. Leibl. 2001. Electron transfer in photosystem I. *Biochim. Biophys. Acta.* 1507:100–114.
13. Savikhin, S. 2006. Ultrafast optical spectroscopy of photosystem I. *In* Photosystem I: The Light-Driven Plastocyanin: Ferredoxin Oxidoreductase. J. Golbeck, ed. Springer, pp. 155–175.
14. Kumazaki, S., I. Ikegami, …, K. Yoshihara. 2001. Observation of the excited state of the primary electron donor chlorophyll (P700) and the ultrafast charge separation in the spinach Photosystem I reaction center. *J. Phys. Chem. B.* 105:1093–1099.
15. Adolphs, J., F. Müh, …, T. Renger. 2010. Structure-based calculations of optical spectra of photosystem I suggest an asymmetric light-harvesting process. *J. Am. Chem. Soc.* 132:3331–3343.
16. Zazubovich, V., S. Matsuzaki, …, G. Small. 2002. Red antenna states of photosystem I from cyanobacterium Synechococcus elongatus: a spectral hole burning study. *Chem. Phys.* 275:47–59.
17. Schlodder, E., F. Lendzian, …, N. V. Karapetyan. 2014. Long-wavelength limit of photochemical energy conversion in Photosystem I. *J. Am. Chem. Soc.* 136:3904–3918.
18. Sumi, H. 2004. Uphill energy trapping by reaction center in bacterial photosynthesis. 2. Unistep charge separation, virtually mediated by special pair, by photoexcitation in place of excitation transfer from the antenna system. *J. Phys. Chem. B.* 108:11792–11801.
19. Gibasiewicz, K., V. Ramesh, …, A. N. Webber. 2001. Excitation dynamics in the core antenna of PSI from *Chlamydomonas reinhardtii* CC 2696 at room temperature. *J. Phys. Chem. B.* 105:11498–11506.
20. Morrison, K. A., A. Akram, …, A. J. Rothnie. 2016. Membrane protein extraction and purification using styrene-maleic acid (SMA) copolymer: effect of variations in polymer structure. *Biochem. J.* 473:4349–4360.
21. Dörr, J. M., S. Scheidelaar, …, J. A. Killian. 2016. The styrene-maleic acid copolymer: a versatile tool in membrane research. *Eur. Biophys. J.* 45:3–21.
22. Knowles, T. J., R. Finka, …, M. Overduin. 2009. Membrane proteins solubilized intact in lipid containing nanoparticles bounded by styrene maleic acid copolymer. *J. Am. Chem. Soc.* 131:7484–7485.

23. Lee, S. C., T. J. Knowles, …, T. R. Dafforn. 2016. A method for detergent-free isolation of membrane proteins in their local lipid environment. *Nat. Protoc.* 11:1149–1162.
24. Orwick-Rydmark, M., J. E. Lovett, …, A. Watts. 2012. Detergent-free incorporation of a seven-transmembrane receptor protein into nanosized bilayer Lipodisq particles for functional and biophysical studies. *Nano Lett.* 12:4687–4692.
25. Sahu, I. D., R. M. McCarrick, …, G. A. Lorigan. 2013. DEER EPR measurements for membrane protein structures via bifunctional spin labels and lipodisq nanoparticles. *Biochemistry.* 52:6627–6632.
26. Gulati, S., M. Jamshad, …, A. J. Rothnie. 2014. Detergent-free purification of ABC (ATP-binding-cassette) transporters. *Biochem. J.* 461:269–278.
27. Swainsbury, D. J., S. Scheidelaar, …, M. R. Jones. 2014. Bacterial reaction centers purified with styrene maleic acid copolymer retain native membrane functional properties and display enhanced stability. *Angew. Chem. Int. Ed. Engl.* 53:11803–11807.
28. Postis, V., S. Rawson, …, S. P. Muench. 2015. The use of SMALPs as a novel membrane protein scaffold for structure study by negative stain electron microscopy. *Biochim. Biophys. Acta.* 1848:496–501.
29. Brady, N. G., M. Li, …, B. D. Bruce. 2019. Non-detergent isolation of a cyanobacterial photosystem I using styrene maleic acid alternating copolymers. *RSC Adv.* 9:31781–31796.
30. Wittig, I., H. P. Braun, and H. Schägger. 2006. Blue native PAGE. *Nat. Protoc.* 1:418–428.
31. Schägger, H., and G. von Jagow. 1991. Blue native electrophoresis for isolation of membrane protein complexes in enzymatically active form. *Anal. Biochem.* 199:223–231.
32. Kubota, H., I. Sakurai, …, H. Wada. 2010. Purification and characterization of photosystem I complex from Synechocystis sp. PCC 6803 by expressing histidine-tagged subunits. *Biochim. Biophys. Acta.* 1797:98–105, Published online September 12, 2009.
33. Ushakov, E., V. Nadtochenko, …, O. M. Sarkisov. 2004. Ultrafast excited state dynamics of the bi-and termolecular stilbene-viologen charge-transfer complexes assembled via host–guest interactions. *Chem. Phys.* 298:251–261.
34. Lorenc, M., M. Ziolek, …, A. Maciejewski. 2002. Artifacts in femtosecond transient absorption spectroscopy. *Appl. Phys. B.* 74:19–27.
35. Homann, C., N. Krebs, and E. Riedle. 2011. Convenient pulse length measurement of sub-20-fs pulses down to the deep UV via two-photon absorption in bulk material. *Appl. Phys. B.* 104:783–791.
36. Dobryakov, A., J. P. Lustres, …, N. Ernsting. 2008. Femtosecond transient absorption with chirped pump and supercontinuum probe: perturbative calculation of transient spectra with general lineshape functions, and simplifications. *Chem. Phys.* 347:127–138.
37. Provencher, S. W. 1982. CONTIN: a general purpose constrained regularization program for inverting noisy linear algebraic and integral equations. *Comput. Phys. Commun.* 27:229–242.
38. Morosinotto, T., J. Breton, …, R. Croce. 2003. The nature of a chlorophyll ligand in Lhca proteins determines the far red fluorescence emission typical of photosystem I. *J. Biol. Chem.* 278:49223–49229.
39. Leupold, D., H. Stiel, and J. Sepiol. 1986. The S1 and T1 spectra of chlorophyll-a in the visible region and an S1-bypassing relaxation from two-photon stepwise excited states. *Chem. Phys. Lett.* 132:137–140.
40. Chauvet, A., N. Dashdorj, …, S. Savikhin. 2012. Spectral resolution of the primary electron acceptor A0 in Photosystem I. *J. Phys. Chem. B.* 116:3380–3386.
41. Joliot, P., and A. Joliot. 1999. In vivo analysis of the electron transfer within photosystem I: are the two phylloquinones involved? *Biochemistry.* 38:11130–11136.
42. Bevington, P. R., D. K. Robinson, …, S. McKay. 1993. Data reduction and error analysis for the physical sciences. *Comput. Phys.* 7:415–416.
43. Shuvalov, V. A. 1976. The study of the primary photoprocesses in photosystem I of chloroplasts. Recombination luminescence, chlorophyll triplet state and triplet-triplet annihilation. *Biochim. Biophys. Acta.* 430:113–121.
44. Savikhin, S., W. Xu, …, W. S. Struve. 2000. Ultrafast primary processes in PS I from Synechocystis sp. PCC 6803: roles of P700 and A(0). *Biophys. J.* 79:1573–1586.
45. Croce, R., and H. van Amerongen. 2013. Light-harvesting in photosystem I. *Photosynth. Res.* 116:153–166.
46. Karapetyan, N. V., Y. V. Bolychevtseva, …, M. Brecht. 2014. Long-wavelength chlorophylls in photosystem I of cyanobacteria: origin, localization, and functions. *Biochemistry (Mosc.).* 79:213–220.
47. Melkozernov, A. N., S. Lin, and R. E. Blankenship. 2000. Excitation dynamics and heterogeneity of energy equilibration in the core antenna of photosystem I from the cyanobacterium Synechocystis sp. PCC 6803. *Biochemistry.* 39:1489–1498.
48. Müller, M. G., C. Slavov, …, A. R. Holzwarth. 2010. Independent initiation of primary electron transfer in the two branches of the photosystem I reaction center. *Proc. Natl. Acad. Sci. USA.* 107:4123–4128.
49. Nürnberg, D. J., J. Morton, …, A. W. Rutherford. 2018. Photochemistry beyond the red limit in chlorophyll f-containing photosystems. *Science.* 360:1210–1213.
50. Yin, S., M. G. Dahlbom, …, J. R. Reimers. 2007. Assignment of the Qy absorption spectrum of photosystem-I from Thermosynechococcus elongatus based on CAM-B3LYP calculations at the PW91-optimized protein structure. *J. Phys. Chem. B.* 111:9923–9930.
51. Gibasiewicz, K., V. M. Ramesh, …, A. N. Webber. 2003. Excitonic interactions in wild-type and mutant PSI reaction centers. *Biophys. J.* 85:2547–2559.
52. Dashdorj, N., W. Xu, …, S. Savikhin. 2004. Electrochromic shift of chlorophyll absorption in photosystem I from Synechocystis sp. PCC 6803: a probe of optical and dielectric properties around the secondary electron acceptor. *Biophys. J.* 86:3121–3130.
53. Shipman, L. L., T. M. Cotton, …, J. J. Katz. 1976. An analysis of the visible absorption spectrum of chlorophyll a monomer, dimer,and oligomers in solution. *J. Am. Chem. Soc.* 98:8222–8230.
54. Gillie, J. K., P. A. Lyle, …, J. H. Golbeck. 1989. Spectral hole burning of the primary electron donor state of Photosystem I. *Photosynth. Res.* 22:233–246.
55. Kurashov, V., M. Gorka, …, J. H. Golbeck. 2018. Critical evaluation of electron transfer kinetics in P700-FA/FB, P700-FX, and P700-A1 Photosystem I core complexes in liquid and in trehalose glass. *Biochim. Biophys. Acta Bioenerg.* 1859:1288–1301.
56. Müller, M. G., J. Niklas, …, A. R. Holzwarth. 2003. Ultrafast transient absorption studies on Photosystem I reaction centers from Chlamydomonas reinhardtii. 1. A new interpretation of the energy trapping and early electron transfer steps in Photosystem I. *Biophys. J.* 85:3899–3922.
57. Riley, K. J., T. Reinot, …, V. Zazubovich. 2007. Red antenna states of photosystem I from cyanobacteria Synechocystis PCC 6803 and Thermosynechococcus elongatus: single-complex spectroscopy and spectral hole-burning study. *J. Phys. Chem. B.* 111:286–292.
58. Giaimo, J. M., A. V. Gusev, and M. R. Wasielewski. 2002. Excited-state symmetry breaking in cofacial and linear dimers of a green perylenediimide chlorophyll analogue leading to ultrafast charge separation. *J. Am. Chem. Soc.* 124:8530–8531.
59. Ihalainen, J. A., M. Rätsep, …, A. Freiberg. 2003. Red spectral forms of chlorophylls in green plant PSI– a site-selective and high-pressure spectroscopy study. *J. Phys. Chem. B.* 107:9086–9093.
60. Cherepanov, D. A., G. E. Milanovsky, …, J. H. Golbeck. 2018. Electron–phonon coupling in cyanobacterial photosystem I. *J. Phys. Chem. B.* 122:7943–7955.